InGaAs Quantum Dots Coupled to a Reservoir of Nonequilibrium Free Carriers

Citation: Gomis-Bresco, J. et al. "InGaAs Quantum Dots Coupled to a Reservoir of Nonequilibrium Free Carriers." Quantum Electronics, IEEE Journal of 45.9 (2009): 1121-1128. © 2009 IEEE

As Published: http://dx.doi.org/10.1109/jqe.2009.2021565

Publisher: Institute of Electrical and Electronics Engineers

Persistent URL: http://hdl.handle.net/1721.1/52416

Version: Final published version: final published article, as it appeared in a journal, conference proceedings, or other formally published context

InGaAs Quantum Dots Coupled to a Reservoir of Nonequilibrium Free Carriers

Jordi Gomis-Bresco, Sabine Dommers, Vasily V. Temnov, Ulrike Woggon, Juan Martinez-Pastor, Matthias Laemmlin, and Dieter Bimberg

***Abstract*—We discuss the impact of a 2-D-charged carrier reservoir for high-speed optical amplification and modulated lasing in quantum dot (QD)-based devices by testing the amplification of short trains of high power, femtosecond optical pulses in an InGaAs QD-in-a-well-based semiconductor optical amplifier (SOA). We adapt a laser-like rate equation model to describe heterodyne pump-and-probe experiments. After an optically induced perturbation, we identify the gain recovery process as a forced steady-state situation which can be consistently described within rate-equation based laser theory. The model is systematically applied to analyze the experimental amplification and the overall SOA dynamics as a function of injected current. We conclude that, under conditions of high optical pump power close to the device saturation regime, the ultrafast SOA dynamics is governed by the overall injection current. The carrier relaxation pathway of a direct capture from the 2–D reservoir to the QD ground state is needed to explain the observed pulse train amplification.**

***Index Terms*—Quantum dot (QD), semiconductor optical amplifier (SOA).**

I. Introduction

QUANTUM DOT (QD)-based devices are key building blocks in future terabit networks. They offer a competitive combination of low-cost and high performance [1] and allow for ultrafast digital signal generation, nonlinear processing and amplification [2]. The physical mechanisms behind gain recovery determine the modulation response of QD-based lasers. Experimental studies at the active medium of a laser under real operation conditions are difficult to perform because the feedback cavity formed by the laser high reflective end-facets prevents single pass optical experiments, otherwise the most appropriate tool. The standard solution is to test active QD-media in semiconductor optical amplifiers (SOAs). An amplifier has the same electronic and waveguide structure as the corresponding laser, but tilted end facets or appropriate coatings avoid back-reflections and thus lasing. In order to study the dynamics in waveguide-structured samples like SOAs, the heterodyne pump and probe technique is a well-established tool [3], [4] and was applied, for example, for studies of the influence of p-doping [5] or of gain and phase dynamics [6] in QD-based devices.

In spite of the fast recovery that QD-based active media exhibit, there are concerns about the successful amplification of pulse trains [7]. Models based on a cascade-like capture under moderate electrical carrier injection predict a dramatic slow down in the gain recovery for the subsequent pulses of a train. Cascade-like carrier capture means that QDs capture carriers through their excited states only. This carrier reservoir is progressively emptied for high-frequency modulation and amplification of optical pulse trains. The gain recovery of the excited state (ES) is significantly slower than the ground state (GS) one [8]. i.e., the excited state-ground state relaxation would then determine the temporal limit for high-frequency operation. This situation could change if the overall dynamics is governed by the injected carrier density in a 2-D-reservoir of a QD-in-a-well structure rather than the average population of high energy excited states [9]. So called DWELL-structures are characterized by a long energy tail in the well density of states (DOS) becoming quasi-resonant to the QD bound states. First results of time resolved photoluminescence experiments in such structures suggested a direct capture from outside the QD (i.e., the 2-D reservoir) directly into the QD ground state [10]. The conditions at which such a direct coupling and capture of 2-D carriers into the QD GS occurs are not studied in detail yet. In particular, the ultrafast dynamics in QD-based systems like active medium of amplifiers and lasers, requires a full microscopic description of the carrier scattering rates [11]–[13]. Under real operating conditions such as strong electrical injection, non-negligible optical pump intensity and elevated temperatures, the time scales of all relaxation processes enter a regime at which polarization and population dynamics contribute equally to the overall ultrafast relaxation dynamics, as has been found, e.g., in four-wave mixing or pump-probe experiments [14], [15]. A variety of theoretical treatments of the dynamics of QD lasers [16]–[19], [11], [12], [20] and SOAs [21]–[23] exist and great efforts go on to connect consistently time constants retrieved from the time-resolved output of the pump and probe experiments and time parameters extracted from the dynamical performance observed in laser experiments [17].

In pump and probe experiments with optical pump pulses of power close to the gain saturation (and simultaneous application of high injection currents), we go beyond the small signal

Manuscript received November 06, 2008; revised March 02, 2009. Current version published August 19, 2009.

J. Gomis-Bresco and U. Woggon are with the Institute of Optics and Atomic Physics, Technical University of Berlin, D-10623 Berlin, Germany.

S. Dommers is with the Physics Department, Technical University of Dortmund, D-44221 Dortmund, Germany.

V. V. Temnov is with the Department of Chemistry, Massachusetts Institute of Technology, Cambridge, MA 02139 USA.

J. Martinez-Pastor is with the Institut de Ciència dels Materials, Universitat de València, Campus Universitario de Paterna, Polígono "La Coma" s/n. 46980 Paterna (Valencia), Spain.

M. Laemmlin and D. Bimberg are with the Institut fuer Festkoerperphysik, Technical University of Berlin, D-10623 Berlin, Germany.

Color versions of one or more of the figures in this paper are available online at http://ieeexplore.ieee.org.

Digital Object Identifier 10.1109/JQE.2009.2021565

amplification regime. Here the situation is more similar to the physical description recently developed to explain relaxation oscillations through a direct capture process from the wetting layer to the QD-bound states [24], [11], [12]. In addition, in some recent works [18], [17] the impact of the thermal population on electron capture rates and thus modulation response of p-doped QD-lasers is analyzed and discussed for application concepts in high-speed SOA and for laser operation.

In this study, we analyze the gain dynamics of InGaAs QDs when they are coupled to a reservoir of nonequilibrium 2-D free carriers by applying simultaneously powerful electrical injection and optical pumping. To emulate the limiting working conditions of modulated lasers we use a SOA with InGaAs QDs-in-a-well embedded in a waveguide structure. We perform heterodyne pump and probe measurements using short trains of high power femtosecond laser pulses, powerful enough to test the optical amplification limits of the active medium. The injection current was varied from 10 to 150 mA and the SOA modulation response measured for pulse trains up to 1 THz optical input frequency.

This paper is organized as follows. After a short description of the sample and the experiment in Section II, we give an overview about the experimental findings after short pulse-train amplification in Section III. In Section IV, we adapt a laser-like rate equation system to the particularities of our experiment. We take into account propagation effects (Subsection IV-A) and we describe the active medium as a population-inverted system forced into a nonequilibrium situation (Subsection IV-B). Section V summarizes the analysis of the experimental findings. We conclude that for the structures presented here, direct capture from the 2-D reservoir to the QD GS is the dominant mechanism to explain the observed pulse train amplification. The applied rate-equation model describes pump and probe experiments as a transient recovery of a steady-state situation following an external optical perturbation. That represents a first step to achieve a consistent agreement between laser theory and experimental rates optically measured.

II. Sample and Experiment

The sample studied in this work is a p-i-n structure with a 1-mm-long, 2-μm-wide waveguide [Fig. 1(a)] (for sample details, see [25]). A deeply etched ridge structure provides strong index guiding of the optical mode and suppression of current spreading [26]. The active medium consists of 15 layers of MBE grown QDs-in-a-well nanostructures with a nominal areal density of $2 \cdot 10^{10}$ cm^{-2} and a nominal delta p-doping of $5 \cdot 10^{17}$ cm^{-2}. A 33–35 nm GaAs spacer ensures strain relaxation between successive layers, in order to achieve a low defect density. As a consequence, electronic coupling between successive QD layers does not occur. Antireflection coating of both end facets avoids lasing and allows single-pass pulse experiments.

Fig. 1(b) shows the amplified spontaneous emission (ASE) of the device at an injection current I_c of 10 and 50 mA. A 33 meV broad (inhomogenous broadening) GS excitonic emission peak is located at $E_{\mathrm{GS}} = 965$ meV ($\lambda = 1.285$ μm) that shifts to 954 meV ($\lambda \simeq 1.3$ μm) with increasing injection current. A well resolved p-shell excited state (ES) emission peak 70 meV above

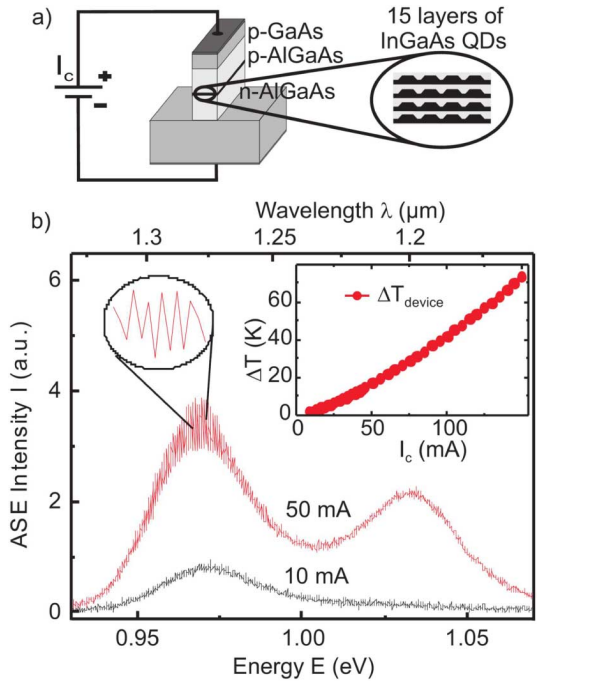

Fig. 1. (a) Sketch of the QD-based SOA. (b) Spectra of the ASE at an injection current I_c of 10 and 50 mA. The inset shows the device temperature ΔT versus I_c inferred from the spectral shifts of the ripple modes.

the ground state dominates at injection currents above 70 mA. The ASE spectra show gain ripple because the antireflection coatings do not fully prevent back reflections in the facets. We have calibrated the thermal dependence of the ripple modes and use it to control the change in the device temperature $\Delta T_{\mathrm{device}}$ as a function of the injection current I_c [inset in Fig. 1(b)].

When we couple light in a facet (ϕ_{in}) of the SOA, it propagates through the device. The light intensity that couples out at the other facet (ϕ_{out}) is either reduced by partial absorption, if the injection current is below transparency current $I_{\mathrm{tr}} = 7.5$ mA, or amplified. The gain of the device is defined as $G = \phi_{\mathrm{in}}/\phi_{\mathrm{out}}$. Gain is calculated based on the transparency current transition, where the SOA offers a gain of $G = 1$. Fig. 2 presents a set of gain curves measured for a single pulse as a function of the in-coupled optical pump power ϕ_{in}. The pump beam has a wavelength resonant to the QD ground state ($\lambda = 1.285$ μm) and an energy per pulse set to $\phi_{\mathrm{in}} = 0.1$ pJ/pulse (dark area in Fig. 2). That energy is in the saturation regime of the device, i.e., the population inversion and the QD volume density are not sufficient to maintain an almost constant gain as for intensities ϕ_{in} below 0.01 pJ/pulse. When working in that regime, we impose a depletion of the population inversion and test the limits of the reservoirs that refill the QDs ground state.

We use femtosecond pump-probe technique with heterodyne detection [15], [4]. The pulses are generated by a Ti:sapphire pumped optical parametric oscillator (OPO). The full-width at half-maximum of the temporal pulse is FWHM = 150 fs and the repetition rate is 75.4 MHz. Using a two-stage Michelson interferometer, we produce pulse trains of up to four pulses with a fixed delay between pulses $\tau_0 = 1$ ps (equivalent to a modulation of 1 THz). The amount of pulses in the train is chosen by blocking/unblocking mirrors in the interferometers. Fig. 3

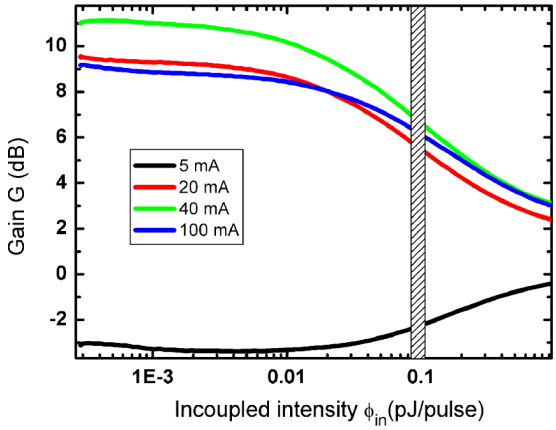

Fig. 2. Gain G as a function of the incoupled light intensity $\phi_{\rm in}$ for single pulse experiments resonant to the QD ground state ($\lambda = 1.28\ \mu$m). The dark area represents the energy per pulse used as the optical pump pulse energy in all pump and probe experiments presented in this work.

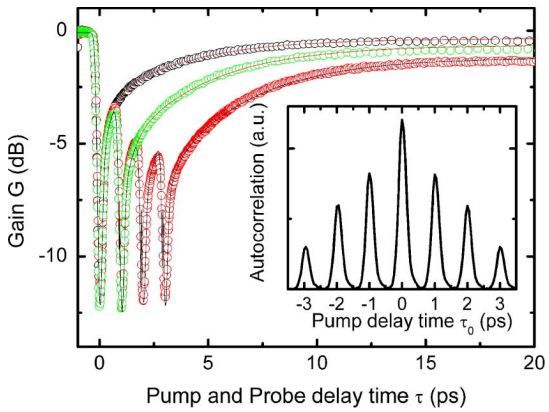

Fig. 3. Time-resolved gain evolution after amplification of one, two, and four pulses at $I_c = 40$ mA. Solid lines correspond to multi-exponential fittings of the experimental data. The inset shows an autocorrelation measurement of a pulse train of four pulses.

shows three pump-probe experiments using 1, 2 or 4 pulses in the optical input pulse train. The time delay τ is defined as the delay between the pump and probe pulses. The inset of Fig. 3 shows an autocorrelation example of the four pulse trains generated.

III. Experimental Results

To understand the mechanisms and limits of optical amplification and ultrafast laser modulation, we perform a systematic experimental study of the gain recovery dynamics in a QD-in-a-well system under strong electrical injection and optical pumping close to gain saturation. Our goal is to obtain a consistent picture of both the injection current dependency of the gain recovery and the response of the QD active medium to a previous amplification process (gain recovery mechanism).

In order to have a first quantitative analysis of the heterodyne pump and probe measurements, we start with a standard fitting expression [4], [27], [28] and apply it to pump and probe data for one, two, and four pulse trains in the gain regime ($I_c =$ 10-150 mA): three exponential decays plus an offset term

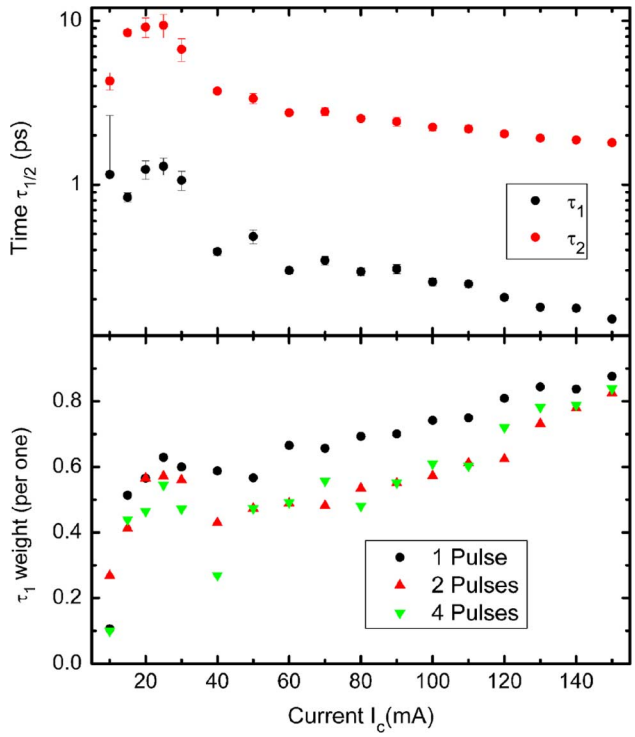

Fig. 4. (a) Time constants τ_1 and τ_2 derived from the fitting as described in the text. (b) Relative weight of the fastest component, τ_1, as a function of injection current I_c.

analytically convoluted to the Gaussian response of the system. The physically interesting time constants retrieved from the fit are the two fastest, τ_1 and τ_2 which are plotted along with their relative weighting in Fig. 4. The slowest component (τ_3) is in the range of QDs radiative lifetime and its relative weight decreases quickly with current, becoming negligible above $I_c =$ 20-30 mA. The results obtained for τ_1 and τ_2 from the fitting routines are plotted in logarithmic scale in Fig. 4(a). For single pulse experiments it holds a relation of $\tau_3 \approx 10 \cdot \tau_2 \approx 100 \cdot \tau_1$ for the retrieved time constants. For $I_c < 30$ mA, i.e., carrier injection currents close to the transparency current $I_{\rm tr}$, τ_1 and τ_2 increase with increasing I_c. In our analysis below, we will show that such a behavior can be assigned to an inhomogeneous absorption process during the propagation of pulses through the waveguide. We will focus therefore on the discussion of results from moderate to high injection currents, $I_c > 30$ mA, i.e., those accelerating the gain recovery, as can be seen in Fig. 4. In that range of $30 < I_c < 40$ mA, both τ_1 and τ_2 decrease strongly with increasing I_c, followed by a nearly constant behavior for $I_c > 60$ mA. In addition, the relative weight of the fastest component (the τ_1 weight) grows until it comprises 90% of the total recovery dynamics at $I_c = 150$ mA.

For the following analysis of the experiments with two and four pulses in the train, we keep τ_1 and τ_2 fixed to the values obtained from the fits of the corresponding single pulse experiments. As can be seen in Fig. 3, all fits, as described above, show good agreement with the experimental data.

For all three experiments with one, two, and four pulses, we find a systematic decrease of τ_1 along with an increase in its

weight when I_c is increased. Therefore, we discuss in the following only that fastest component τ_1 relative weight, as presented in Fig. 4(b). We can state from the experiment that an increase (decrease) of τ_1 relative weight corresponds to a speed up (slow down) of the gain recovery dynamics. Under conditions of powerful electrical injection, the τ_1 relative weight reduces only gradually after amplification, even if the power per pulse used is sufficient to fully deplete the GS population inversion (see Section II). τ_1 weight decreases slowly from single-pulse to double-pulse experiments and remains almost unchanged when comparing two- and four-pulse train dynamics. The microscopic background of that τ_1 time constant is nonlinear Coulomb scattering in a thermal nonequilibrium situation and subject of further investigation which will be presented elsewhere.

IV. Model

Our goal in this work is to adapt the rate-equation description developed for lasers and amplifiers to the description of heterodyne pump and probe measurements under conditions of moderate to strong optical pumping and simultaneous electrical carrier injection. We are interested in a quantitative model of the gain recovery dynamics in the time range of a few picosecond, i.e., the typical time scale of Coulomb scattering times [13], [12]. We neglect the very early femtosecond dynamics on time scales of the incoming temporal pulse widths as well as the very long dynamics on time scales of carrier recombination. In order to get a qualitative description of the ultrafast gain recovery, we developed a simple rate-equation model based on the carrier population evolution of the confined QD levels and the higher energy levels (sum up in a general 2-D reservoir level). Using it, we emphasize the peculiarities of the experimental scheme, given here.

- *Propagation effects in the waveguide*. The strength of the incoming pulse grows during guided propagation under gain operation and, as a consequence, the population depletion is highly inhomogenous.
- The pump and probe experiment is described as a *return to the steady-state situation in an* electrically *inverted system* after being perturbed by an external electromagnetic field.

A. Propagation Effects

Accounting for the inhomogeneous absorption profile, we include propagation effects in the model as described in the following: We divide the waveguide into 200 slices, each 5 μm long, perpendicular to the propagation direction. Given an incoming photon flux at slice z_n, we calculate the temporal population evolution and the resulting outcoming photon flux $(\phi(t, z_{n+1}))$. Afterwards we use that propagated and amplified photon flux as incoming pulse for the next slice z_{n+1}.

We consider two different photon fluxes, pump $(\phi_{\rm pu}\ (t, z_n))$ and probe $(\phi_{\rm pr}(t, z_n, \tau))$. The initial pump photon flux $\phi_{\rm pu}(0, z_n)$ consists of a sum of temporal gaussians resembling the experiment. The first Gaussian is centered at $t = 0$ and sets the time origin of the simulation.

In order to simulate the characteristics of the optical pulse trains, several Gaussians with different relative delay times between them are used. $\phi_{\rm pr}(0, z_n, \tau)$, the initial probe photon flux, consists of a single Gaussian centered at $t = \tau$, the delay between pump and probe pulses. For fix delays τ in the interval $\tau = [-1, 8]$, we calculate 30 ps (from $\mathrm{t} = -1$ ps to $\mathrm{t} = 29$ ps) of the temporal evolution for all 200 slices, following the integration procedure sketch in Fig. 5.

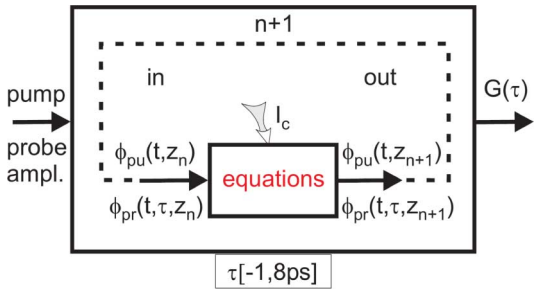

Fig. 5. Diagram of the iterative numerical treatment used in the proposed model (for details, see the text).

The experimental outcome of a pump and probe measurement is the gain (or absorption) experienced by the probe beam. We calculate the gain $G(\tau)$, defined as

$$G(\tau) = \frac{\phi_{\rm pr}(\mathrm{n} \cdot l, z_{200}, \tau)}{\phi_{\rm pr}(0, z_0, \tau)} \tag{1}$$

where n is the refractive index of GaAs and l is the length of the device, that is, we calculate the ratio between the propagated and the initial probe beams as a function of delay time τ.

The result is a normalized gain quantity $G_{\rm norm}$ that can be directly compared with the experimental gain curves, once they are normalized.

B. Inverted System Returning to a Steady-State Situation

The population inversion in the QD system is set by the injection current applied, i.e., at a given I_c the carrier distribution in the system is determined by the *steady-state equilibrium* between the capture, escape, spontaneous and stimulate radiative rates among the energy levels. That forced thermal equilibrium induced by I_c remains stable and unchanged as long as I_c remains fixed. The short pulse of the pump beam perturbs that equilibrium and forces the electrically inverted population out of the steady-state situation. The pump and probe experiment monitors then the return process to the steady-state situation. In our simulations, we first calculate the steady-state populations without external light propagating through the device for a given fixed injection current I_c. Afterwards, we calculate the temporal evolution of the pump and probe experiment setting the initial conditions at every slice to that of the steady-state populations.

A first simplification in our model is the choice of a rate-equation model instead of semiconductor QD Bloch equations to describe the QD system. We consider only the population dynamics and disregard the coupled polarization evolution. This is partly justified when concentrating on a qualitative estimate of the picosecond dynamic range.

We define two subensembles of QDs with their GS and ES energy levels either resonant (rs) or nonresonant (nrs) to the degenerate pump and probe energy. The percentage of rs-QDs is obtained from the overlap of the ASE and the pulse spectrum.

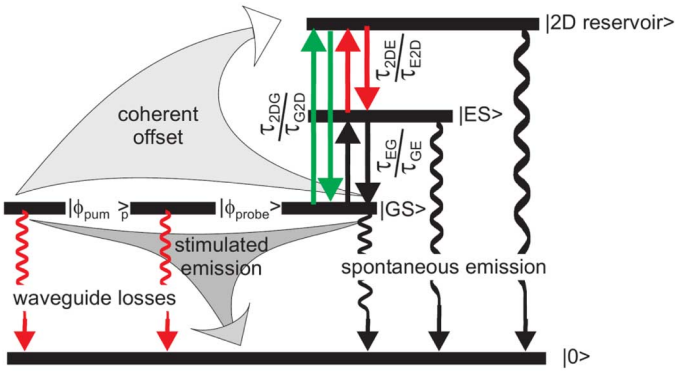

Fig. 6. Scheme of the InGaAs QD-in-a-well based SOA energy states included in the modeling.

Both sub-ensembles are formally isolated, but they can be thermally connected through the 2-D reservoir that they share. The p-doping in the device leads to an excess of holes near the QD and a hole built-in population in the QDs [29]; so we assume that the overall dynamics is governed only by electrons. We write different populations equations for both subensembles $(n_{G,E}^{\mathrm{rs,nrs}})$. The core of our system is described by the following equation system:

$$\begin{aligned}\frac{dn_{2\mathrm{D}}}{dt} &= I_{\mathrm{ec}} + S_{\mathrm{G2D}} n_G^{\mathrm{rs,nrs}} - S_{2\mathrm{DG}} \left(2N_{\mathrm{QDs}} - n_G^{\mathrm{rs,nrs}}\right) \\ &\quad + S_{\mathrm{E2D}} n_E^{\mathrm{rs,nrs}} - S_{2\mathrm{DE}} \left(4N_{\mathrm{QDs}} - n_E^{\mathrm{rs,nrs}}\right) \\ &\quad - S_{\mathrm{r2D}} n_{2\mathrm{D}}. \end{aligned} \tag{2}$$

$$\begin{aligned}\frac{dn_E^{\mathrm{rs,nrs}}}{dt} &= S_{2\mathrm{DE}} \left(4N_{\mathrm{QDs}} - n_E^{\mathrm{rs,nrs}}\right) - S_{\mathrm{E2D}} n_E^{\mathrm{rs,nrs}} \\ &\quad - S_{\mathrm{EG}} n_E^{\mathrm{rs,nrs}} \left(1 - \frac{n_G^{\mathrm{rs,nrs}}}{2N_{\mathrm{QDs}}}\right) \\ &\quad + S_{\mathrm{GE}} n_G^{\mathrm{rs,nrs}} \left(1 - \frac{n_E^{\mathrm{rs,nrs}}}{4N_{\mathrm{QDs}}}\right) - S_r n_E^{\mathrm{rs,nrs}}. \end{aligned} \tag{3}$$

$$\begin{aligned}\frac{dn_G^{\mathrm{rs,nrs}}}{dt} &= S_{2\mathrm{DG}} \left(2N_{\mathrm{QDs}} - n_G^{\mathrm{rs,nrs}}\right) - S_{\mathrm{G2D}} n_G^{\mathrm{rs,nrs}} \\ &\quad - S_{\mathrm{GE}} n_G^{\mathrm{rs,nrs}} \left(1 - \frac{n_E^{\mathrm{rs,nrs}}}{4N_{\mathrm{QDs}}}\right) \\ &\quad + S_{\mathrm{EG}} n_E^{\mathrm{rs,nrs}} \left(1 - \frac{n_G^{\mathrm{rs,nrs}}}{2N_{\mathrm{QDs}}}\right) - S_r n_E^{\mathrm{rs,nrs}} \\ &\quad + S_{\phi G} \left(n_G^{\mathrm{rs}} - N_{\mathrm{QDs}}\right) \phi - S_{\mathrm{coh}} n_G^{\mathrm{rs}} \phi. \end{aligned} \tag{4}$$

$$\frac{d\phi}{dz} = S_{\phi G} \left(n_G^{\mathrm{rs}} - N_{\mathrm{QDs}}\right) \phi - S_{\mathrm{coh}} n_G^{\mathrm{rs}} \phi - \alpha\phi. \tag{5}$$

$n_G^{\mathrm{rs,nrs}}$, $n_E^{\mathrm{rs,nrs}}$, $n_{2\mathrm{D}}$ are the electron population of GS, ES and the 2-D reservoir, respectively. N_{QDs} is the total amount of QDs in the considered volume and ϕ refers to the total photon flux that travels through the device. Term I_{ec} stands for the effective injected current expressed as the real amount of carriers injected in the QD-2-D reservoir system in contrast to the full current injected to the device I_c.

Fig. 6 presents a diagram of the levels considered in our model. The physical processes represented by arrows in Fig. 6 are included in the differential equation system as rates ($\mathrm{S_{InitialFinal}}$, with Initial, Final = G(GS), E(ES) and 2D(2D Reservoir)). The exact calculation of the scattering rates involves a microscopic approach that takes into account the instantaneous carrier density of the levels implied and can be found, e.g., in [11]–[13]. Here we define effective times τ related to the rates S and use them as free parameters during the fitting procedure to experimental data. Since we are essentially interested in the dynamics within the first few picoseconds after the pulse, coherent phenomena occurring during and shortly after the pump pulse arrival are approximated here as an offset term (S_{coh}) in the rate equations, proportional to the photon flux (ϕ). This simplification is based on the small dephasing times (T_2) that QDs present at temperatures equal or higher than room temperature [14], [15].

S_r is the inverse of the GS and ES radiative lifetime τ_r (assumed to be the same for GS and ES), while $S_{r2\mathrm{D}}$ is the inverse of the effective residence time $\tau_{2\mathrm{D}}$ in the 2-D reservoir.

Capture rates from the 2-D to the GS (ES), $S_{2\mathrm{DG}(E)}$, depend on the available electron population in the 2-D reservoir $(n_{2\mathrm{D}})$. In rate equation models focused in small signal and injected current regimes, this term is expressed as $(n_{2\mathrm{D}})/(\tau_{2\mathrm{DG}(E)} \epsilon N_{\mathrm{QDs}})$, where $\epsilon = 2, 4$ for GS and ES respectively and $\tau_{2\mathrm{DG}(E)}$ stands for the 2-D to GS(ES) capture time. But at high currents, the term results in rates greater than one $(n_{2\mathrm{D}} \gg N_{\mathrm{QDs}})$, so we approximate the terms by

$$S_{2\mathrm{DG}} = \frac{1}{\tau_{2\mathrm{DG}}} \left(1 - e^{\frac{-n_{2D}}{2N_{\mathrm{QDs}}}}\right) \tag{6}$$

$$S_{2\mathrm{DE}} = \frac{1}{\tau_{2\mathrm{DE}}} \left(1 - e^{\frac{-n_{2D}}{4N_{\mathrm{QDs}}}}\right) \tag{7}$$

that tend to become close to 1 when $n_{2\mathrm{D}} \gg N_{\mathrm{QDs}}$, but recover the standard form for $n_{2\mathrm{D}} \ll N_{\mathrm{QDs}}$.

The thermal redistribution of carriers is taken into account through the escape rates, $S_{G(E)2D}$ and S_{GE}. We relate them to the capture rates by introducing the Boltzmann factor $e^{(\Delta E_{\mathrm{InitialFinal}})/(k_B T_c)}$, where T_c is the carrier temperature and not the device temperature [30]–[32]:

$$S_{\mathrm{G2D}} = \frac{1}{\tau_{2\mathrm{DG}}} e^{\frac{\Delta E_{G2D}}{k_B T_c}} \tag{8}$$

$$S_{\mathrm{E2D}} = \frac{1}{\tau_{2\mathrm{DE}}} e^{\frac{\Delta E_{E2D}}{k_B T_c}} \tag{9}$$

$$S_{\mathrm{GE}} = \frac{1}{\tau_{\mathrm{EG}}} e^{\frac{\Delta E_{\mathrm{GE}}}{k_B T_c}}. \tag{10}$$

These terms lead to the forced thermal steady-state situation described at the beginning of this section.

Finally, the amplification/absorption rate $S_{\phi G}$ is expressed as

$$S_{\phi G} = \left(1 - e^{g \cdot \phi}\right) \tag{11}$$

where g stands for the gain per slice of width dz. The term recovers the usual form $(g \cdot \phi)$ for $\phi \ll N_{\mathrm{QDs}}$ and does not give an amplification rate bigger than n_G (when multiplied by the rest of the term) for high photon fluxes, allowing us to reproduce the high photon flux regime used in our experiments.

V. Results and Discussion

Here, the rate-equation model outlined in Section IV is applied to the systematic analysis of the gain dynamics of single-, double-, and four-pulse experiments for input pulse repetition

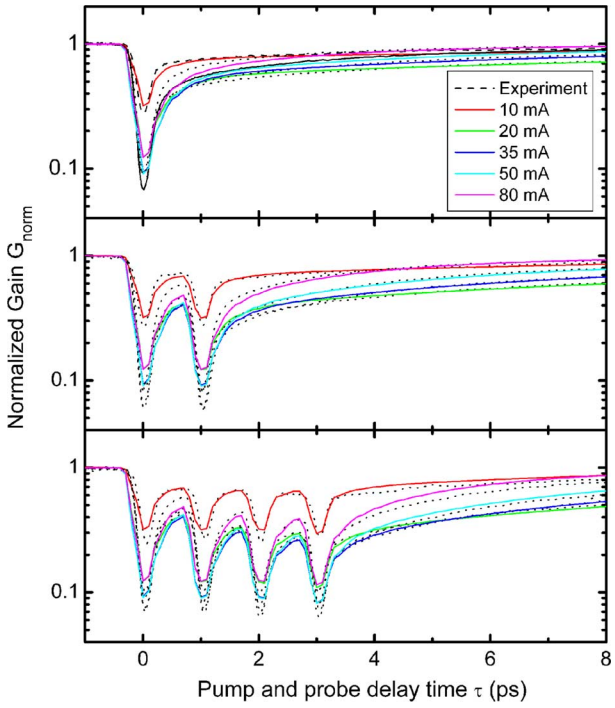

Fig. 7. Normalized gain curves as a function of I_c measured for one, two, and four pulses in the train. Solid lines show the corresponding model simulations.

rates up to 1 THz. In experiments with multiple pulses, we chose experimental conditions at which the power per pulse at a fixed I_c is equal for all pulses of the incoming pulse train. Consequently, we can fit groups of data (one-, two-, and four-pulse curves measured at the same I_c) with a shared parameter set in a global least-squared minimization routine. That restricts the fit to consistent parameter values capable of reproducing the after-pulse dynamics observed.

Part of the parameters (lower part of Table I) used in the simulation are determined by the experimental conditions. We divide the analysis of the experimental data in two rounds. In a first round, we fit the data for a fixed $I_c = 35$ mA and determine the best fit parameter (Fig. 7). An overview about the parameter set obtained in that first round is given in Table I. After discussing these parameters, we fit in a second round the results of the remaining applied I_c-values based on that first round fitting result.

Fast capture times $\tau_{2\mathrm{DG}}$ and $\tau_{2\mathrm{DE}}$, that is, constant relaxation times from the 2-D reservoir to the GS and ES, are similar to the retrieved τ_1 parameter, the fast component of the multi-exponential fitting routine performed before and shown in Fig. 4 of Section III. This implies in the rate equation description, i.e., under neglection of the polarisation and focussing on the population dynamics, an equivalence of the fastest time constant with a direct capture rate from the 2-D reservoir to the QD bound states. While this might be a reasonable first approximation, we point here to the fact that scattering rate calculations, made for similar 2-D reservoir carrier densities, predicted slightly slower values for those processes [24]. In a future analysis, the impact of microscopic scattering processes on the dephasing times and thus on the overall SOA dynamics has to be included to reduce the observed discrepancies and to uncover the microscopic scattering mechanisms. However, the most remarkable result we can

TABLE I
BEST FIT (UPPER PANEL) AND AB INITIO FIXED (LOWER PANEL) PARAMETERS USED TO FIT THE EXPERIMENTAL NORMALIZED GAIN AT FIXED $I_c = 35$ MA (FIG. 7). $\tau_{\mathrm{InitialFinal}}$, WHERE Initial, Final = G (GS), E (ES) AND 2D (2D RESERVOIR) ARE THE TIME CONSTANTS ASSOCIATED TO THE PROCESS CONNECTING THE INITIAL AND FINAL ENERGY LEVELS. $\Delta \mathrm{E}_{\mathrm{InitialFinal}}$, IS THE ENERGY SPLITTING BETWEEN THE INITIAL AND FINAL ELECTRON LEVELS

Parameter	Value (Units)
τ_{2DG},τ_{2DE}	100 fs
τ_{EG}	500 fs
τ_{rG}, τ_{rE}	445 ps
τ_{r2D}	0.7 ps
Effective injected current I_{ec}	5 mA
Carrier temperature T_c	403 K
$\Delta \mathrm{E}_{EG}$	45 meV
$\Delta \mathrm{E}_{2DG}$	210 meV
g (gain in 5μm)	0.125 photons^{-1}
waveguide losses α	5 cm^{-1}
Pump Intensity	0.1 pJ per pulse
Probe Intensity	0.001 pJ per pulse

provide from the analysis here, lies in the fact that a fast $\tau_{2\mathrm{DG}}$ constant is mandatory to reproduce the experimental gain recovery of several pulse trains. The progressive slow-down predicted after a multiple train pulse [7] reduces when we consider in addition a direct capture to the QD ground state. The time constant τ_{EG}, the carrier relaxation time in the QD, is larger than $\tau_{2\mathrm{DG}}$ and $\tau_{2\mathrm{DE}}$. This fact tells us again that scattering processes involving carriers not confined at the QD are dominant.

Finally, we would like to emphasize, that the variation of the temperature is important for obtaining a satisfying fit which is a clear hint to a thermal nonequilibrium situation. The obtained values lie above the device temperature (Fig. 1), as one might expect for an electrically pumped system which needs further studies. Possibly in pulsed experiments at short times, below the recombination lifetime, thermalization is not complete and $T_{\mathrm{carriers}} > T_{\mathrm{equilibrium}}$ holds in the device.

The time constants τ_{rG} and τ_{rE} are compatible with typical QD radiative lifetimes, but their values could be affected by the amplified process that a spontaneous emission suffers in a waveguide. The fitting also yields that only $\sim$15% (I_{ec}/I_c) of the injected current is entirely captured (transferred) in(to) the QD 2-D reservoir system. The main parameter to reproduce the experimental variation of I_c is, obviously, the effective injected current I_{ec}.

The variation of the injection current I_c has further impacts in the device properties.

- The device temperature depends on I_c, as shown in Fig. 1 and drives the carrier temperature T_c into a nonequilibrium situation.
- The carrier effective residence time in the 2-D reservoir τ_{r2D} depends on current-induced carrier drifts and related changes in the wetting layer degeneracy that is a function of temperature too [18].
- I_c affects $\tau_{2\mathrm{DG}}$, $\tau_{2\mathrm{DE}}$ and τ_{EG} through changes of the carrier densities (n_G, n_E and $n_{2\mathrm{D}}$).

To have closer look on the influence of I_c on the experimental results, we simulate the gain curves for different injection currents I_c with only three free parameters: I_{ec}, T_c and τ_{r2D} whereas $\tau_{2\mathrm{DG}}$, $\tau_{2\mathrm{DE}}$ and τ_{EG} are fixed to the values found for $I_c = 35$ mA (Table I). Fits to one, two, and four pulse trains are shown in Fig. 7 for several injection currents. We can see how

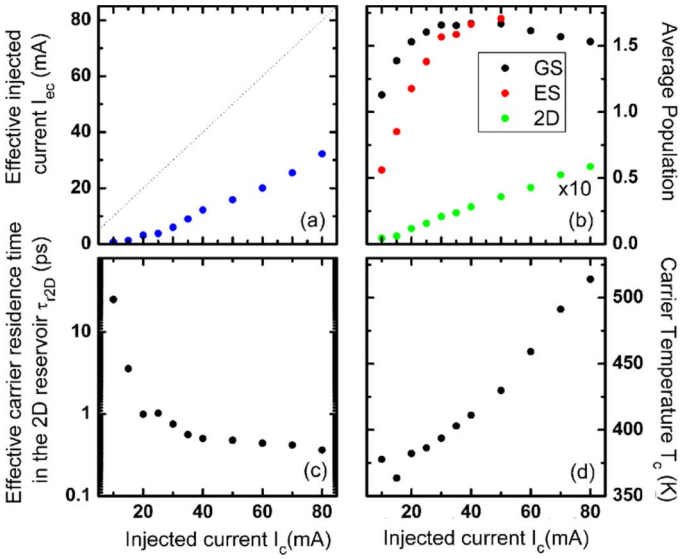

Fig. 8. (a) Effective injected current $I_{\rm ec}$ (scattered points). (b) Average population per QD in the system (n_G, n_E and $n_{\rm 2D}$). (c) Effective lifetime in the 2-D reservoir $\tau_{\rm r2D}$. (d) Carrier temperature T_c, versus the experimental injected current I_c to the device. Dashed dot line in (a) is an eye-guideline $y = I_c$.

our model is able to explain satisfactory the pulse amplification process by the studied SOA by only taking into account experimental data from ultrafast experiments and a small number of parameters representing the effective operation in our device. Note, that the model does not correctly reproduce the first half picosecond after a pulse because we omitted coherent effects from the beginning and treated them as a simple coherent offset. A more detailed discussion of that very early time regime can be found in [33] based on semiconductor quantum dot Bloch equations and specific T_2 measurements as a function of I_c.

Fig. 8 presents the best-fit parameters of our systematic analysis. It shows that our model is able to give us other valuable information, like the average population in thermal equilibrium, i.e., before the optical pump pulse arrival (pump and probe delay $\tau < 0$). Likewise we get access to the average population of the ground state n_G which grows with current, but saturates at 1.5 excitons per dot (2 is the maximum degeneracy of the GS). The thermal carrier redistribution reduces the maximum gain available [34]. The general trend of the data confirms that the dynamics is governed by the overall injected current rather than by the average population of the high energy levels. As expected, we can describe qualitatively the normalized gain evolution by adjusting the injected current and the effects it has on the device, mainly carrier temperature [Fig. 8(d)], that grows more than the measured lattice temperature (Fig. 1(b) inset) as corresponds to an electrically pumped system, and the effective carrier residence time in the 2-D reservoir [Fig. 8(c)] that reduces as current grows.

Summarizing, we performed and analyzed heterodyne pump and probe experiments at InGaAs QDs-in-a-well SOAs using small trains of high-power pulses, powerful enough to test the amplification limits of the active medium. We adapt a laser-like rate-equation model to describe the population dynamics as a recovery process of a forced steady-state situation after an optical induced perturbation. Our results show that temperature and its effects on the device become crucial to understand and model the active medium dynamics. From our analysis, we conclude that the relaxation dynamics of a InGaAs QDs-in-a-well SOA operated at high injection currents and close to gain saturation is sufficiently fast to amplify pulse combs up to several hundreds of gigahertz.

REFERENCES

[1] D. Mowbray and M. Skolnick, "New physics and devices based on self-assembled semiconductor quantum dots," *J. Phys. D: Appl. Phys.*, vol. 38, no. 13, pp. 2059–2076, Jul. 7, 2005.

[2] D. Bimberg, G. Fiol, M. Kuntz, C. Meuer, M. Laemmlin, and N. N. Ledentsov, "High speed nanophotonic devices based on quantum dots," *Phys. Status Solidi A*, vol. 203, no. 14, pp. 3523–3532, Nov. 2006.

[3] K. Hall, G. Lenz, E. Ippen, and G. Raybon, "Heterodyne pump probe technique for time-domain studies of optical nonlinearities in waveguides," *Opt. Lett.*, vol. 17, no. 12, pp. 874–876, Jun. 15, 1992.

[4] K. Hall, G. Lenz, A. Darwish, and E. Ippen, "Subpicosecond gain and index nonlinearities in InGaAs p diode-lasers," *Opt. Commun.*, vol. 111, no. 5–6, pp. 589–612, Oct. 15, 1994.

[5] V. Cesari, W. Langbein, P. Borri, M. Rossetti, A. Fiore, S. Mikhrin, I. Krestnikov, and A. Kovsh, "Ultrafast gain dynamics in 1.3 μm InAs/GaAs quantum-dot optical amplifiers: The effect of p doping," *Appl. Phys. Lett.*, vol. 90, no. 20, p. 201103, May 14, 2007.

[6] T. Vallaitis, C. Koos, R. Bonk, W. Freude, M. Laemmlin, C. Meuer, D. Bimberg, and J. Leuthold, "Slow and fast dynamics of gain and phase in a quantum dot semiconductor optical amplifier," *Opt. Exp.*, vol. 16, no. 1, pp. 170–178, Jan. 7, 2008.

[7] T. Berg, S. Bischoff, I. Magnusdottir, and J. Mork, "Ultrafast gain recovery and modulation limitations in self-assembled quantum-dot devices," *IEEE Photon. Technol. Lett.*, vol. 13, no. 6, pp. 541–543, Jun. 2001.

[8] S. Schneider, P. Borri, W. Langbein, U. Woggon, R. Sellin, D. Ouyang, and D. Bimberg, "Excited-state gain dynamics in InGaAs quantum-dot amplifiers," *IEEE Photon. Technol. Lett.*, vol. 17, no. 10, pp. 2014–2016, Oct. 2005.

[9] K. Veselinov, F. Grillot, C. Cornet, J. Even, A. Bekiarski, M. Gioannini, and S. Loualiche, "Analysis of the double laser emission occurring in 1.55-μm InAs-InP(113)B quantum-dot lasers," *IEEE J. Quantum Electron.*, vol. 43, no. 9-10, pp. 810–816, Sep.–Oct. 2007.

[10] G. Rainò, G. Visimberga, A. Salhi, M. De Vittorio, A. Passaseo, R. Cingolani, and M. De Giorgi, "Simultaneous filling of InAs quantum dot states from the GaAs barrier under nonresonant excitation," *Appl. Phys. Lett.*, vol. 90, no. 11, p. 111907, Mar. 12, 2007.

[11] E. Malic, K. J. Ahn, M. J. P. Bormann, P. Hoevel, E. Schoell, A. Knorr, M. Kuntz, and D. Bimberg, "Theory of relaxation oscillations in semiconductor quantum dot lasers," *Appl. Phys. Lett.*, vol. 89, no. 10, p. 101107, Sep. 4, 2006.

[12] E. Malic, M. J. P. Bormann, P. Hoevel, M. Kuntz, D. Bimberg, A. Knorr, and E. Schoell, "Coulomb damped relaxation oscillations in semiconductor quantum dot lasers," *IEEE J. Sel. Top. Quantum Electron.*, vol. 13, no. 5, pt. 1, pp. 1242–1248, Sep.–Oct. 2007.

[13] T. Nielsen, P. Gartner, and F. Jahnke, "Many-body theory of carrier capture and relaxation in semiconductor quantum-dot lasers," *Phys. Rev. B*, vol. 69, no. 23, p. 235314, Jun. 2004.

[14] P. Borri, W. Langbein, S. Schneider, U. Woggon, R. Sellin, D. Ouyang, and D. Bimberg, "Rabi oscillations in the excitonic ground-state transition of InGaAs quantum dots," *Phys. Rev. B*, vol. 66, no. 8, p. 081306, Aug. 15, 2002.

[15] P. Borri, W. Langbein, S. Schneider, U. Woggon, R. Sellin, and D. Ouyang, "Exciton relaxation and dephasing in quantum-dot amplifiers from room to cryogenic temperature," *IEEE J. Sel. Top. Quantum Electron.*, vol. 8, no. 5, pp. 984–991, Sep.–Oct. 2002.

[16] P. Bhattacharya, S. Ghosh, S. Pradhan, J. Singh, Z. Wu, J. Urayama, K. Kim, and T. Norris, "Carrier dynamics and high-speed modulation properties of tunnel injection InGaAs-GaAs quantum-dot lasers," *IEEE J. Quantum Electron.*, vol. 39, no. 8, pp. 952–962, Aug. 2003.

[17] W. Chow and S. Koch, "Theory of semiconductor quantum-dot laser dynamics," *IEEE J. Quantum Electron.*, vol. 41, no. 4, pp. 495–505, Apr. 2005.

[18] D. Deppe and H. Huang, "Fermi's golden rule, nonequilibrium electron capture from the wetting layer, and the modulation response in p-doped quantum-dot lasers," *IEEE J. Quantum Electron.*, vol. 42, no. 3–4, pp. 324–330, Mar.–Apr. 2006.

[19] A. Fiore and A. Markus, "Differential gain and gain compression in quantum-dot lasers," *IEEE J. Quantum Electron.*, vol. 43, no. 3–4, pp. 287–294, Mar.–Apr. 2007.
[20] C. Meuer, J. Kim, M. Laemmlin, S. Liebich, A. Capua, G. Eisenstein, A. R. Kovsh, S. S. Mikhrin, I. L. Krestnikov, and D. Bimberg, "Static gain saturation in quantum dot semiconductor optical amplifiers," *Opt. Expr.*, vol. 16, no. 11, pp. 8269–8279, May 26, 2008.
[21] T. Berg and J. Mork, "Quantum dot amplifiers with high output power and low noise," *Appl. Phys. Lett.*, vol. 82, no. 18, pp. 3083–3085, May 5, 2003.
[22] T. Berg and J. Mork, "Saturation and noise properties of quantum-dot optical amplifiers," *IEEE J. Quantum Electron.*, vol. 40, no. 11, pp. 1527–1539, Nov. 2004.
[23] T. Berg, J. Mork, and J. Hvam, "Gain dynamics and saturation in semiconductor quantum dot amplifiers," *New J. Phys.*, vol. 6, p. 178, Nov. 26, 2004.
[24] K. Lüdge, M. J. P. Bormann, E. Malic, P. Hövel, M. Kuntz, D. Bimberg, A. Knorr, and E. Schöll, "Turn-on dynamics and modulation response in semiconductor quantum dot lasers," *Phys. Rev. B*, vol. 78, p. 035316, 2008.
[25] S. Dommers, V. V. Temnov, U. Woggon, J. Gomis, J. Martínez-Pastor, M. Laemmlin, and D. Bimberg, "Complete ground state gain recovery after ultrashort double pulses in quantum dot based semiconductor optical amplifier," *Appl. Phys. Lett.*, vol. 90, no. 3, p. 033508, Jan. 15, 2007.
[26] M. Kuntz, G. Fiol, M. Lammlin, D. Bimberg, M. Thompson, K. Tan, C. Marinelli, A. Wonfor, R. Sellin, R. Penty, I. White, V. Ustinov, A. Zhukov, Y. Shernyakov, A. Kovsh, N. Ledentsov, C. Schubert, and V. Marembert, "Direct modulation and mode locking of 1.3 μm quantum dot lasers," *New J. Phys.*, vol. 6, p. 181, Nov. 26, 2004.
[27] P. Borri, W. Langbein, J. Hvam, E. Heinrichsdorff, M. Mao, and D. Bimberg, "Ultrafast gain dynamics in InAs-InGaAs quantum-dot amplifiers," *IEEE Photon. Technol. Lett.*, vol. 12, no. 6, pp. 594–596, Jun. 2000.
[28] P. Borri, W. Langbein, J. Hvam, F. Heinrichsdorff, M. Mao, and D. Bimberg, "Spectral hole-burning and carrier-heating dynamics in InGaAs quantum-dot amplifiers," *IEEE J. Sel. Top. Quantum Electron.*, vol. 6, no. 3, pp. 544–551, May–Jun. 2000.
[29] K. Sun, A. Kechiantz, B. Lee, and C. Lee, "Ultrafast carrier capture and relaxation in modulation-doped inas quantum dots," *Appl. Phys. Lett.*, vol. 88, no. 16, pp. 163117–, Apr. 17, 2006.
[30] H. Jiang and J. Singh, "Nonequilibrium distribution in quantum dots lasers and influence on laser spectral output," *J. Appl. Phys.*, vol. 85, no. 10, pp. 7438–7442, May 15, 1999.
[31] A. Markus, J. Chen, O. Gauthier-Lafaye, J. Provost, C. Paranthoen, and A. Fiore, "Impact of intraband relaxation on the performance of a quantum-dot laser," *IEEE J. Sel. Top. Quantum Electron.*, vol. 9, no. 5, pp. 1308–1314, Sep.–Oct. 2003.
[32] A. Bilenca and G. Eisenstein, "On the noise properties of linear and nonlinear quantum-dot semiconductor optical amplifiers: The impact of inhomogeneously broadened gain and fast carrier dynamics," *IEEE J. Quantum Electron.*, vol. 40, no. 6, pp. 690–702, Jun. 2004.
[33] J. Gomis-Bresco, D. Dommers, V. Temnov, U. Woggon, M. Laemmlin, D. Bimberg, E. Malic, M. Richter, E. Schoell, and A. Knorr, "Impact of Coulomb scattering on the ultrafast gain recovery in InGaAs quantum dots," *Phys. Rev. Lett.*, vol. 101, p. 256803, Dec. 19, 2008.
[34] D. Matthews, H. Summers, P. Smowton, and M. Hopkinson, "Experimental investigation of the effect of wetting-layer states on the gain-current characteristic of quantum-dot lasers," *Appl. Phys. Lett.*, vol. 81, no. 26, pp. 4904–4906, Dec. 23, 2002.

Jordi Gomis-Bresco received the Diploma and the Ph.D. degree in physics from the University of Valencia, Valencia, Spain, in 2002 and 2008, respectively.

He was scientific employee with the Technical University of Dortmund, Dortmund, Germany, and the Technical University of Berlin, Berlin, Germany, where he is currently employed. His current research interests are focused on ultrafast spectroscopy of semiconductor quantum dots and single-dot spectroscopy.

Sabine Dommers received the Diploma in physics from the Technical University of Dortmund, Dortmund, Germany, in 2005, where she is currently working towards the Ph.D. degree.

Her current research interests are focused on ultrafast spectroscopy.

Vasily Temnov received the Diploma in theoretical quantum optics from the University of Essen, Essen, Germany, in 1999 and the Ph.D. degree from the University of Duisburg-Essen, Duisburg, Germany, in 2004. His doctoral work focused on experimental studies of ultrafast laser-induced phenomena in solids.

In 2005, he joined the Technical University of Dortmund, Dortmund, Germany, as a Postdoctoral Associate, working in the field of nanooptics. In 2008, he joined Massachusetts Institute of Technology, Cambridge, as the German Science Foundation research fellow specializing on ultrafast plasmonics.

Ulrike Woggon recieved the Diploma in physics and the Ph.D. degree from the Humboldt University, Humboldt, Germany, in 1982 and 1985, respectively, and the habilitation degree from the University of Kaiserslautern in 1995 for her work on optical properties of semiconductor quantum dots.

From 1997 to 2008, she held a Full University Professorship (C3) for Experimental Physics with the Technical University of Dortmund, Dortmund, Germany. Since 2008, she has been a Full University Professor with the Institute of Optics and Atomic Physics at the Technical University of Berlin, Berlin, Germany. Her current research interests are focused on ultrafast spectroscopy of semiconductor quantum dots, single-dot spectroscopy, and quantum dots in microcavities and other photonic materials.

Juan Martinez-Pastor received the degree and the Ph.D. in physics From the University of Valencia in 1985 and 1990, respectively.

He is a Full Professor of Applied Physics at the University of Valencia. He is specialized in Semiconductor Physics, particularly optical properties of quantum heterostructures and nanostructures based on III-V semiconductors. He developed postdoctoral stays at the European Laboratory of Non Linear Spectroscopy, Florence, Italy, and at the Ecole Normale Suprieure, Paris, France, for two and one years, respectively.

Matthias Laemmlin received the M.S. degree from the University of Massachusetts at Amherst in 1999, the Diploma degree in physics from the Universitaet Konstanz, Konstanz, Germany, in 2000, and the Ph.D. degree from the Technical University of Berlin, Berlin, Germany, on quantum-dot based semiconductor optical amplifiers in 2006.

His research interests include photonic device physics and characterization techniques, with emphasis on nanotechnology in opto-electronics.

Dieter Bimberg received the Diploma in physics and the Ph.D. degree from Goethe University, Frankfurt, Germany, in 1968 and 1971, respectively.

From 1972 to 1979, he held a Principal Scientist position at the Max-Planck-Institute for Solid State Research in Grenoble/France and Stuttgart. In 1979, he was appointed as a Professor of Electrical Engineering with the Technical University of Aachen, Aachen, Germany. Since 1981 he has held the Chair of Applied Solid State Physics with the Technical University of Berlin (TU Berlin), Berlin, Germany. Since 1990, he has been the Excecutive Director of the Solid State Physics Institute at TU Berlin. Since 2004, he has been the director of the Center of Nanophotonics at TU Berlin. In 2006 he was elected as chairman of the German National Centers of Excellence of Nanotechnologies. His research interests include the physics of nanostructures and photonic devices, like quantum dot lasers and amplifiers, single photon emitters, wide-gap semiconductor heterostructures, and ultrahigh-speed photonic devices.